Molecular Orientation Distributions in Uniaxially Oriented Poly(L-lactic acid) Films Determined by Polarized Raman Spectroscopy

Masakazu Tanaka and Robert J. Young*

Materials Science Centre, School of Materials, The University of Manchester, Grosvenor Street, Manchester, M1 7HS, U.K.

Received December 8, 2005; Revised Manuscript Received March 7, 2006

ABSTRACT: Molecular orientation distributions in the crystalline and amorphous regions were studied for uniaxially oriented poly(L-lactic acid) (PLLA) films using polarized Raman spectroscopy. By combining wide-angle X-ray diffraction and birefringence measurements, the tilt angle between the principal axis of the Raman tensor and the molecular chain axis was determined for Raman bands assigned to the crystalline regions only, and also to those being independent of morphology. The changes of the molecular orientation distribution functions during the drawing were analyzed in detail. The PLLA molecules in the crystalline regions were found to be highly oriented at a draw ratio of 4.5, probably as a result of crystal rotation and crystal slip. In contrast, the development of molecular orientation in the amorphous regions appeared to take place by pseudo-affine deformation. The results suggest that the film needs to be stretched to draw ratios above 4.5 to achieve successful molecular orientation in the amorphous regions.

1. Introduction

Poly(L-lactic acid) (PLLA) is a biodegradable polyester synthesized chemically from L-lactic acid monomers, which are renewable in nature.[1−3] PLLA has been used as a biomaterial[4−6] owing to its biocompatibility. In addition, the packaging industry has been investigating the potential of PLLA as an eco-friendly material[1−3] owing to its renewability.

The macroscopic properties of PLLA materials depend largely on their crystalline and amorphous microstructures,[7−10] and in particular on the degree of crystallinity. In addition, the degree of molecular orientation also influences physical properties of the material such as its mechanical strength,[6,11] thermal shrinkage,[10] and degradation rate.[8,11] It is, therefore, important to characterize the molecular orientation in both the crystalline and amorphous regions of the material in order to understand the microstructure−property relationships.

The degree of molecular orientation and their distributions can be determined quantitatively by using the orientation distribution function,[12−14] $N(\phi,\theta,\psi)$, given by

$$N(\phi,\theta,\psi) = \sum_{l=0}^{\infty}\sum_{m=-}^{l}\sum_{ln=-l}^{l}\frac{N_{lmn}}{4\pi^2}P_{lmn,\mathrm{chain}}Z_{lmn}(\cos\theta)\mathrm{e}^{-\mathrm{i}m\psi}\mathrm{e}^{-\mathrm{i}n\phi}$$

$$N(\phi,\theta,\psi) = \frac{1}{4\pi^2}\sum_{lmn}N_{lmn}P_{lmn,\mathrm{chain}}Z_{lmn}(\cos\theta)\mathrm{e}^{-\mathrm{i}m\psi}\mathrm{e}^{-\mathrm{i}n\phi} \quad (1)$$

where ϕ, θ, and ψ are Euler angles, $P_{lmn,\mathrm{chain}}$ is the *molecular orientation distribution coefficient* of the order *lmn*, $Z_{lmn}(\cos\theta)$ is an expansion coefficient, and N_{lmn} is calculated for the order *lmn* by,[14]

$$N_{lmn}{}^2 = N_{l\bar{m}n}{}^2 = N_{lm\bar{n}}{}^2 = N_{l\bar{m}\bar{n}}{}^2 = \frac{2l+1}{2}\frac{(l+m)!(l-n)!}{(l-m)!(l+n)!}\frac{1}{[(m-n)!]^2} \quad (2)$$

A number of techniques have been used for the determination of molecular orientation in PLLA materials. Sample birefringence[15−17] and wide-angle X-ray diffraction[18−20] (WAXD) are useful to quantify the molecular orientation averaged over the sample and in the crystalline regions only, respectively, whereas it is difficult to use these techniques to obtain information about the molecular orientation in the amorphous regions. Solid ^{13}C nuclear magnetic resonance (^{13}C NMR) has been applied[21] for the analysis of uniaxially oriented PLLA films, although this technique requires costly instrumentation and complicated data interpretation.[22,23]

Infrared[24] (IR) and Raman spectroscopy[10,25,26] have the potential to quantify the molecular orientation distributions in both the crystalline and amorphous regions using vibrational bands that correspond to these regions. While IR dichroism measurements[27] can determine the molecular orientation distribution coefficients of the order $l = 2$ only, polarized Raman spectroscopy[28,29] can determine the coefficients of both the orders $l = 2$ and 4, which may be further useful to estimate[30] the coefficients of the order $l = 6$. It is, however, important to note that the orientation distribution coefficients obtained from IR and Raman bands initially provide information about the orientation of the dipole moment and the Raman polarizability, respectively, and their relation to the molecular orientation is often ignored.[31]

The authors have introduced a new approach[32] of using polarized Raman spectroscopy for the study of molecular orientation distributions in both the crystalline and amorphous regions of polymeric materials. This method distinguishes Raman bands assigned to the crystalline regions only from ones that are independent of the crystalline and amorphous

* Corresponding author: Telephone: +44-161-306-3551. Fax: +44-161-306-3586. E-mail: robert.young@manchester.ac.uk.

10.1021/ma0526286 CCC: $33.50
Published on Web 04/08/2006

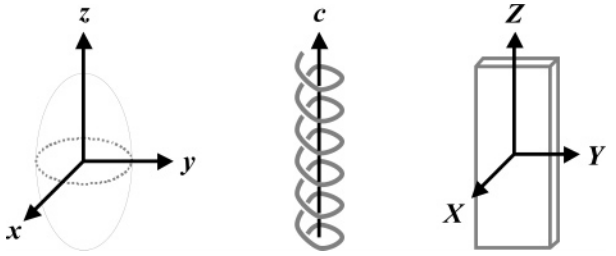

Figure 1. Definitions of the coordinates for a cylindrical Raman tensor ($x-y-z$), the molecular chain axis (c), and the specimen ($X-Y-Z$).

morphology of PLLA by observing the temperature dependence of the Raman spectra.

In this paper, the assignments of Raman bands to the morphology of PLLA were carried out prior to the study of the molecular orientation distributions of uniaxially oriented PLLA films. Assuming that all the Raman bands have cylindrical symmetry as a result of the helical molecular conformation of PLLA, the tensor forms of the Raman bands and the tilt angle, Ω, which is the angle between the cylindrical symmetry axis of the Raman tensor and the molecular chain axis, were determined. The molecular orientation distribution coefficients have been determined for the crystalline and amorphous regions of the PLLA film, to provide information about the different deformation process for the crystalline and amorphous regions. Finally, the change of molecular orientation distributions with sample draw ratio in the necked region of a uniaxially oriented PLLA film was followed successfully using polarized Raman spectroscopy.

2. Principles

The principles of polarized Raman spectroscopy for the study of molecular orientation distributions in both the crystalline and amorphous regions of polymeric materials are summarized briefly in the following section, and the details are given elsewhere.[32]

2.1. Form of Raman Tensor. The axes and coordinate system used in this study are summarized in Figure 1. The coordinates for a cylindrical Raman tensor are given by the *x*-, *y*-, and *z*-axes, with the *z*-axis being set to be along its symmetry axis. The molecular chain axis is defined as the *c*-axis. The specimen coordinates are given by the *X*-, *Y*-, and *Z*-axes, and with the *Z*-axis being set to be along the draw axis of the film.

PLLA molecules form a 10_3 helical structure in the α-form crystal,[33,34] and the helix may be retained in the amorphous regions as reported[35] for similar isotactic polypropylene molecules with a 3_1 helix. Raman tensors of a molecule with molecular symmetry $C_{10/3}$ were assumed to be cylindrically symmetric, and they can be classified[32,36] into the following four types: A($k+$), A($k-$), E(III) and E(V).

The Raman tensors are considered to be oriented uniaxially in the drawing direction of uniaxially oriented PLLA films, and this can reduce the number of nonzero orientation distribution coefficients, P_{200} and P_{400} only, to be determined. The relative intensities of polarized Raman scattering for three independent polarization scattering geometries can be used[32,36] to calculate the P_{200} and P_{400} values for each form of Raman tensor. Subsequently, the tensor form of a Raman band can be determined[32] by comparing the relative intensities with additional information about the sign of the P_{200} value as shown in Table 1.

2.2. Determination of the Molecular Orientation Distribution Coefficients in Both the Crystalline and Amorphous Regions. The orientation distribution coefficient P_{l00} for the Raman tensor with cylindrical symmetry can be correlated[37−40] with the molecular orientation distribution coefficient, $P_{l00,\mathrm{chain}}$, by considering their angular relationship in the following equation

$$P_{l00,\mathrm{chain}} = \frac{P_{l00}}{P_{l00}(\cos \Omega)} \tag{3}$$

where Ω is the so-called "tilt angle" , which is the angle between the cylindrical symmetry axis (*z*-axis) of the Raman tensor and the molecular chain axis (*c*-axis), and the functions $P_{l00}(\cos \Omega)$ are Legendre polynomial functions[41] of cos Ω.

Some of the Raman bands of PLLA have been assigned[10,42−44] to its crystalline regions only. Once the tilt angle Ω of one of the Raman bands is known, the molecular orientation distribution coefficients for the crystalline regions only, $P_{l00,\mathrm{c}}$, can be determined from the P_{l00} values for the Raman tensor using eq 3. Conversely, the tilt angle Ω of the Raman tensor can be determined[32] from the coefficients $P_{l00,\mathrm{c}}$, which are obtained[45,46] using WAXD by

$$P_{l00,\mathrm{c}} = \frac{\int_0^{\pi} N(\theta) P_{l00}(\cos \theta) \sin \theta \, \mathrm{d}\theta}{\int_0^{\pi} N(\theta) \sin \theta \, \mathrm{d}\theta} \tag{4}$$

where θ is an azimuthal angle.

On the other hand, the P_{l00} values for the amorphous regions, $P_{l00,\mathrm{a}}$, can be determined[32] by combining the P_{l00} values for the Raman band that are independent of the morphology, the degree of crystallinity, χ_{c}, and sample birefringence, Δn, using the following relationship

$$\frac{2}{3\cos^2\Omega - 1} P_{200} = \chi_{\mathrm{c}}\left(1 - \frac{\Delta n_{\mathrm{c}}}{\Delta n_{\mathrm{a}}}\right) P_{200,\mathrm{c}} + \frac{\Delta n}{\Delta n_{\mathrm{a}}} \tag{5}$$

where Δn_{c} and Δn_{a} are the values of intrinsic birefringence for the crystalline and amorphous regions of PLLA, respectively. The tilt angle Ω for a "morphology-independent" Raman band of PLLA can be determined from the slope of the plots of the P_{200} values against the right-hand term in eq 5.

Subsequently, the $P_{200,\mathrm{a}}$ value can be determined using the following equation,[47−49]

$$\Delta n = \chi_{\mathrm{c}} P_{200,\mathrm{c}} \Delta n_{\mathrm{c}} + (1 - \chi_{\mathrm{c}}) P_{200,\mathrm{a}} \Delta n_{\mathrm{a}} \tag{6}$$

If the $P_{200,\mathrm{a}}$ value is positive, the $P_{400,\mathrm{a}}$ value could further be estimated[50] from the following equation:

Table 1. Scheme for the Determination of the Form of a Raman Tensor Obtained by Using Correlations between Polarized Raman Scattering Intensities for Different Polarization Geometries[32]

maximum intensity[a]	intensity correlation	the sign of the P_{200} value	form of Raman tensor	tilt angle (Ω)
I_{YY}	$I_{YY} > I_{YZ} \sim I_{ZZ}$		E(V)	Ω < 45°
	$I_{YY} > I_{ZZ} > I_{YZ}$	$P_{200} > 0$	A($k+$)	Ω < 45°
		$P_{200} < 0$	A($k-$)	Ω > 45°
I_{YZ}	$I_{YZ} > I_{YY} \sim I_{ZZ}$	$P_{200} > 0$	E(III)	Ω < 45°
		$P_{200} < 0$	E(III)	Ω > 45°
I_{ZZ}	$I_{ZZ} > I_{YY}$		E(V)	Ω > 45°
	$I_{ZZ} > I_{YY} > I_{YZ}$	$P_{200} > 0$	A($k-$)	Ω < 45°
		$P_{200} < 0$	A($k+$)	Ω > 45°

[a] I_{IJ} signifies the polarized Raman scattering intensity for which incident and scattered lights are polarized in the *I*-axis and *J*-axis directions, respectively.

$$P_{400,a} = \frac{P_{200,a}(5P_{200,a} - 2)}{5 - 2P_{200,a}} \quad (7)$$

2.3. The Most Probable Molecular Orientation Distribution Function. The distribution of the uniaxial molecular orientation can be described using the *molecular orientation distribution function*,[51,52] $N(\theta)$, which is correlated with the P_{l00} values by

$$N(\theta) = \sum_{l=0}^{\infty}\left(\frac{2l+1}{2}\right)P_{l00}\,P_{l00}(\cos\theta) \quad (8)$$

All the P_{l00} values should be determined in order to know the function $N(\theta)$, although polarized Raman spectroscopy can provide the P_{l00} values for the orders $l = 2$ and 4 only.

On the basis of information entropy theory,[53,54] the contributions of the terms for the P_{l00} values of the orders l higher than 4 in eq 8 can be taken into account by replacing eq 8 to the *most probable molecular orientation distribution function*, $N_{mp}(\theta)$, which is defined[26,53,54] by the following equation

$$N_{mp}(\theta) = \frac{\exp[A_{200}^{mp}P_{200}(\cos\theta) + A_{400}^{mp}P_{400}(\cos\theta)]}{\int_0^{\pi}\exp[A_{200}^{mp}P_{200}(\cos\theta) + A_{400}^{mp}P_{400}(\cos\theta)]\sin\theta\,d\theta} \quad (9)$$

where the parameters A_{l00}^{mp} can be calculated numerically under the following constraint:

$$P_{l00} = \frac{\int_0^{\pi} N_{mp}(\theta)P_{l00}(\cos\theta)\sin\theta\,d\theta}{\int_0^{\pi} N_{mp}(\theta)\sin\theta\,d\theta} \quad (10)$$

A program was written using the "solver" function of software Microsoft Excel, to determine the values of A_{200}^{mp} and A_{400}^{mp} for a given set of the P_{200} and P_{400} values.

3. Experimental Section

3.1. Materials. PLLA granules (EcoPla 3010D, Cargill-Dow) were used as the PLLA material throughout this study. The granules were melted at 195 °C and compression-molded into a film with 0.4 mm thickness under a pressure of 2.8 MPa. Subsequently, an isotropic amorphous PLLA film was obtained by quenching (at ca. 20 °C/min) in press cooled with running water. On the other hand, an isotropic crystalline film was obtained by switching off the power and leaving the specimen in press until the temperature fell to room temperature (at ca. 10 °C/h) without the water-cooling. The appearance of the amorphous PLLA film was transparent, while that of the crystalline film was translucent. The difference in film opacity is considered to be due to the difference in sample crystallinity, since differential scanning calorimetry showed 0% and 48% crystallinity for the amorphous and crystalline films, respectively. The isotropy of both the crystalline and amorphous films were confirmed by birefringence measurements that indicated no sample birefringence.

A uniaxially drawn PLLA film was prepared by deforming the amorphous film. A 40 mm × 5 mm strip was cut from the film, and stretched uniaxially at a deformation speed of 10%/min at 75 ± 0.5 °C in an air oven. When the drawing process was completed, the film was taken immediately out of the oven and cooled to room temperature. A photographic image of the sample is shown in Figure 2. The local draw ratio was determined by measuring the distance between lines marked on the strip prior to the drawing. The film has a gradient in draw ratio (DR) from 1.2 up to the final draw ratio of DR = 4.5 in areas A1−A8, respectively, as listed in Table 2.

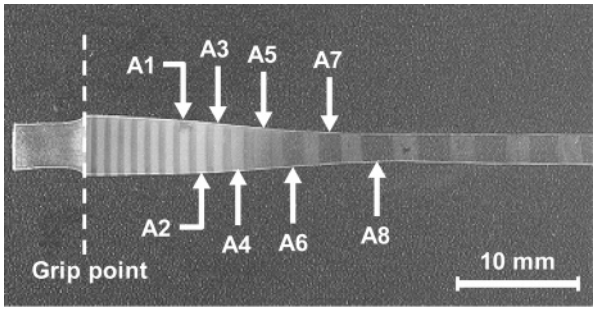

Figure 2. Photograph of the necked PLLA film (final DR = 4.5) by uniaxial drawing for the study of molecular orientation distributions. A*i* indicates the local areas focused on in the study.

Table 2. Draw Ratios (DR), the Degrees of Crystallinity (χ_c), and Estimated Birefringence Values (Δn) in the Local Areas (Figure 2) of the PLLA Film after drawing

area	DR	χ_c	Δn ($\times 10^{-3}$)
A1	1.2	0.42	12.1
A2	1.3	0.39	16.2
A3	1.3	0.40	15.8
A4	1.8	0.41	19.3
A5	2.3	0.40	24.1
A6	2.9	0.36	30.0
A7	3.3	0.41	31.6
A8	4.5	0.49	33.5

In addition, fully uniaxially drawn films with different draw ratios were prepared from the amorphous strips using the same equipment and conditions, but changing the deformation speed to 100%/min. By application of different amounts of elongation, uniaxially oriented PLLA films with draw ratios (DR) between 4.2 and 27.0 were obtained.

3.2. Methods. 3.2.1. Polarized Raman Spectroscopy. A Raman spectrometer (Raman Imaging microscope System 1000, Renishaw) fitted with a near-IR laser (λ = 785 nm, 22 mW output) was employed for the present study. The Raman scattered light was collected through an objective lens (×50, NA = 0.75), and the intensity was recorded using a charge-coupled device (CCD) camera in the backscattering geometry.[55] The effect of the objective lens on the polarization crambling[29,56−59] of Raman scattering was assumed to be insignificant owing to the nature of the sample showing small birefringence.

For the assignment of the Raman bands of PLLA to its crystalline and amorphous regions, Raman spectra of the amorphous PLLA film were obtained at different temperatures from 25 to 200 °C. The film was heated on a hot stage (THMS 600, TMS 91, Linkam), and held at controlled conditions (±1 °C) for 5 min prior to the collection of the spectra.

For the measurement of polarized Raman scattering intensities, polarized Raman spectra were obtained for three different polarization geometries: $X(ZZ)X$, $X(YZ)X$ and $X(YY)X$ (according to Porto's notation[60]) at room temperature. The spectra were analyzed using analytical software (GRAMS/32, Galactic), and the Raman peak was fitted to a Gaussian−Lorentzian function[31] to improve the accuracy of the intensity measurement. The spectrometer and its polarization efficiency were calibrated using a silicon crystal and liquid carbon tetrachloride in order to correct the polarized Raman scattering intensity. The scattering intensity was determined from an average of five replicated measurements.

3.2.2. Wide-Angle X-ray Diffraction (WAXD). The orientation distributions of PLLA crystallites in the drawn film were studied by means of WAXD. Ni-filtered Cu Kα radiation (40 kV, 40 mA) from an X-ray generator (PW 1120/90, Philips) was focused on local areas of the film using a collimator with a pinhole diameter of 0.65 mm. A flat-plate camera was employed to record the diffraction patterns using appropriate exposure times.

The X-ray film negatives were scanned using a digital scanner (Scan Jet ADF, Hewlett-Packard), and the images were analyzed using X-ray analytical software (Fit 2D, ESRF[61]).

The orientation distribution coefficient of crystallites, $P_{200,c}$ were calculated from the diffraction patterns for the (110) and (200) planes of the PLLA α-form crystals. The averaged cosine of the angle between the crystal *c*-axis and the film *Z*-axis, $\langle\cos^2\theta_{c,Z}\rangle$, can be correlated[45] with those of the angles between the normal vectors of the (110) plane and the *Z*-axis, $\langle\cos^2\theta_{110,Z}\rangle$, and between the normal vector of the (200) plane and the *Z*-axis, $\langle\cos^2\theta_{200,Z}\rangle$, by

$$\langle\cos^2\theta_{c,Z}\rangle = 1 - \langle\cos^2\theta_{110,Z}\rangle - \langle\cos^2\theta_{200,Z}\rangle \tag{11}$$

since the *c*-axis is perpendicular to both the normal vectors of the (110) and (200) planes. The PLLA molecules are packed in a pseudohexagonally in the α-form crystal;[33,34] hence,

$$\langle\cos^2\theta_{110,Z}\rangle = \langle\cos^2\theta_{200,Z}\rangle \tag{12}$$

The value of $\langle\cos^2\theta_{110,Z}\rangle$ can be calculated from

$$\langle\cos^2\theta_{110,Z}\rangle = \frac{\int_0^{\pi} I_{110}(\theta)\cos^2\theta\sin\theta\,\mathrm{d}\theta}{\int_0^{\pi} I_{110}(\theta)\sin\theta\,\mathrm{d}\theta} \tag{13}$$

where $I_{110}(\theta)$ is the diffraction intensity distribution along the azimuthal angle θ. Once the value of $\langle\cos^2\theta_{c,Z}\rangle$ is known, the $P_{200,c}$ value can be calculated[45] by

$$P_{200,c} = \frac{3\langle\cos^2\theta_{c,Z}\rangle - 1}{2} \tag{14}$$

3.2.3. Birefringence Measurement. A polarized microscope (BH2, Olympus), which was equipped with a monochromatic filter ($\lambda = 549$ nm), a Senármont compensator and a rotational analyzer, was employed for the measurement of sample birefringence (Δn) of the uniaxially oriented films. The film thickness was measured under the microscope after embedding the film into an epoxy resin (Epofix, Streuer) and obtaining the film cross-section by polishing. The film thickness and the Δn value were determined from an average of five replicated measurements.

3.2.4. Differential Scanning Calorimetry (DSC). A differential scanning calorimeter (2920 MDSC, TA Instruments) was employed to measure the degree of crystallinity, χ_c, of each local area of the drawn film. Heat flow of the sample was recorded between 25 and 200 °C at a ramp rate of 10 °C/min, and an integral of the melting endotherm, ΔH_m, was obtained to calculate the χ_c value using the following equation

$$\chi_c = \frac{\Delta H_m}{\Delta H_c} \tag{15}$$

where ΔH_c is the heat of fusion (93.3 J/g) of a PLLA α-form crystal with an infinite size.[62] The χ_c value was determined from averaging two replicated measurements, and the results are given in Table 2. The increase in the degree of crystallinity during the drawing process is considered to be due to annealing[7,63] and orientation-induced crystallization.[64]

4. Results and Discussion

4.1. Assignments of Raman Bands and Their Depolarization Ratio. Raman spectra of the isotropic crystalline PLLA film obtained at 25 and 200 °C are shown in Figure 3. It can be seen that the weak Raman bands at 1222, 926, 510, and 347 cm^{-1} were not present at 200 °C. Since the melting point of PLLA α-form crystals has been reported to be around 175 °C,[33,65] these Raman bands were assigned to the crystalline regions only of PLLA. This was confirmed by an observation that these Raman bands increased their intensities when the molten sample was recystallized at 110 °C for 30 min. On the other hand, the rest of the Raman bands were observed at both

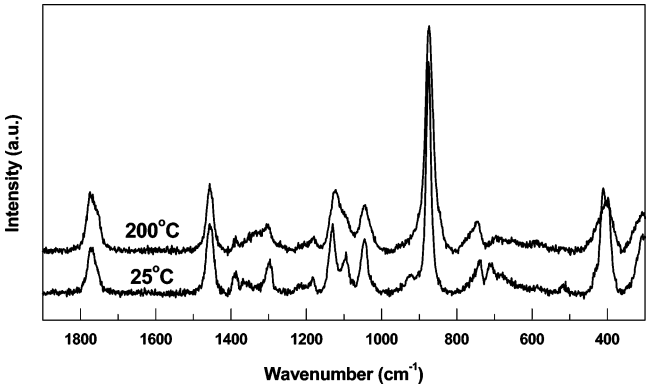

Figure 3. Raman spectra of an isotropic crystalline PLLA film at 25 and 200 °C.

25 and 200 °C; hence, these Raman bands are considered to be independent of the morphology of PLLA. The results are summarized in Table 3 and are shown to be comparable with reports in the literature.[10,42,43,66]

Figure 4 shows polarized Raman spectra of the amorphous PLLA film for two different polarization geometries in order to determine the depolarization ratio (ρ_{iso}) of the Raman bands using

$$\rho_{iso} = \frac{I_{normal}}{I_{parallel}} \tag{16}$$

where $I_{parallel}$ and I_{normal} are the scattering intensities, for which the polarization direction of the analyzed beam is parallel and normal to that of the incident beam, respectively. The ρ_{iso} value for each Raman band is given in Table 3. For the Raman bands assigned to the crystalline regions of PLLA, their ρ_{iso} values were difficult to determine due to their low intensities. The ρ_{iso} values for these Raman bands were, therefore, determined from the spectra of the isotropic crystalline PLLA film, and are given in Table 3.

Possible tensor classes for the Raman bands of PLLA are suggested based on these ρ_{iso} values, and are given in Table 3. The current results are consistent with the literature,[44] although the classes are not clear for the Raman bands with a ρ_{iso} value close to 0.75.

4.2. Determination of the Tensor Forms for the Raman Bands of PLLA. Figure 5 shows the polarized Raman spectra for area A8 of the drawn PLLA film for different polarization scattering geometries. The intensities of the scattering peaks were compared for each Raman band, and are summarized in Table 4. Peaks are overlapped with those of their neighboring Raman bands for the bands at 1767, 1753, 1302, 1295, and 347 cm^{-1}; hence, it was difficult to measure their peak intensities. The signs of the P_{200} and P_{400} values were calculated from the spectra in Figure 5 for all the possible tensor forms, and are given in Table 4.

The scheme shown in Table 1 was applied to determine the tensor form of the Raman bands of PLLA. As a result, Raman bands at 1457, 1099, 875, and 398 cm^{-1} were assigned to the A($k-$) tensor form; those at 926 and 510 cm^{-1} were assigned to the E(III) tensor form; and Raman band at 1222 cm^{-1} was assigned to the *E*(*V*) Raman tensor. Although the rest of the Raman bands could be assigned either to the A($k+$) or A($k-$) form, no further information was obtained to determine their tensor form.

For the Raman bands for which their tensor forms are known, the P_{200} values were calculated from the polarized Raman

Table 3. Assignments of Raman Bands to the Crystalline and Amorphous Regions of PLLA, Their Depolarization Ratio, and Possible Class[a]

	band assignment			depolarization ratio and class			
Raman band (cm^{-1})	current study	Kister et al.[42,43]	Qin et al.[66]	ρ_{iso} (amorphous)	ρ_{iso} (crystalline)	possible class	class[43]
1777	Cr/Am	Cr/Am	/	0.22	/	A	/
1767	Cr/Am	Cr/Am	Am	0.30	/	A	/
1753	Am > Cr	Cr/Am	/	0.41	/	A	A
1457	Cr/Am	Cr/Am	/	0.83	/	E	A, E
1302	Cr/Am	Cr/Am	/	0.74	/	A, E	E
1295	Cr ≫ Am	Cr/Am	/	W	0.71	A, E	A
1222	Cr	Cr/Am	Cr > Am	W	0.79	E	E
1186	Cr/Am	Cr/Am	Cr > Am	0.25	/	A	A
1133	Cr/Am	Cr/Am	/	0.21	/	A	A
1099	Cr ≫ Am	Cr/Am	Cr > Am	0.65	/	A	A, E
1047	Cr/Am	Cr/Am	/	0.50	/	A	A
926	Cr	Cr	/	W	0.93	E	E
875	Cr/Am	Cr/Am	/	0.16	/	A	A
740	Cr ≫ Am	Cr/Am	Cr > Am	W	0.27	A	A
713	Cr ≫ Am	Cr	Cr > Am	W	0.35	A	A
510	Cr	Cr	Cr	W	0.74	A, E	E
413	Cr > Am	Cr/Am	/	W	0.34	A	A
398	Cr/Am	Cr/Am	/	0.78	/	A, E	E
347	Cr	Cr	/	W	0.32	A	A

[a] Key: (Cr) crystalline regions; (Am) amorphous regions; (Cr/Am) independent of morphology; (Am > Cr) more significant in the amorphous regions; (Cr > Am) more significant in the crystalline regions; (/) not determined; (W) difficult to determine the ρ_{iso} value due to weak intensities.

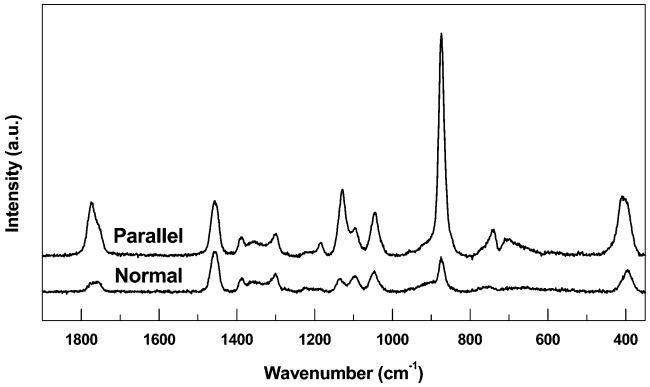

Figure 4. Polarized Raman spectra of an isotropic amorphous PLLA film. For the parallel and normal polarization geometries, the polarization direction of the analyzed beam was either parallel or normal to that of the incident beam, respectively.

spectra for the areas from A1 to A8, and they are plotted against the local draw ratios in Figure 6. A monotonic increase of the P_{200} values was observed for the Raman bands at 1222, 926, and 510 cm^{-1}. This implies that in the areas of higher local draw ratios the tensor *z*-axis of these Raman bands become oriented more toward the direction of the uniaxial drawing. In contrast, there was a monotonic decrease of the P_{200} values for Raman bands at 1457, 1099, and 398 cm^{-1}; in other words, the *z*-axes of these Raman bands were tilted away from the film drawing direction as the film was drawn uniaxially. This suggests that the *z*-axes of the Raman bands have their tilt angles more than 45° away from the molecular chain axis (*c*-axis).

4.3. Tilt Angle for the Raman Bands Assigned to the Crystalline Regions Only. X-ray fiber patterns were obtained for areas from A1 to A8 of the drawn PLLA film, and those for areas A2, A4, A6, and A8 are shown in Figure 7. A pair of intense diffraction arcs in the equatorial direction were assigned to the (110) and (200) planes, while those in the meridional direction were assigned to the (0,0,10) and (1,0,10) planes of PLLA α-form crystals.[33,34] The change of these diffraction patterns indicates that the *c*-axes of the crystallites become aligned preferentially toward the film drawing direction with increasing local draw ratio.

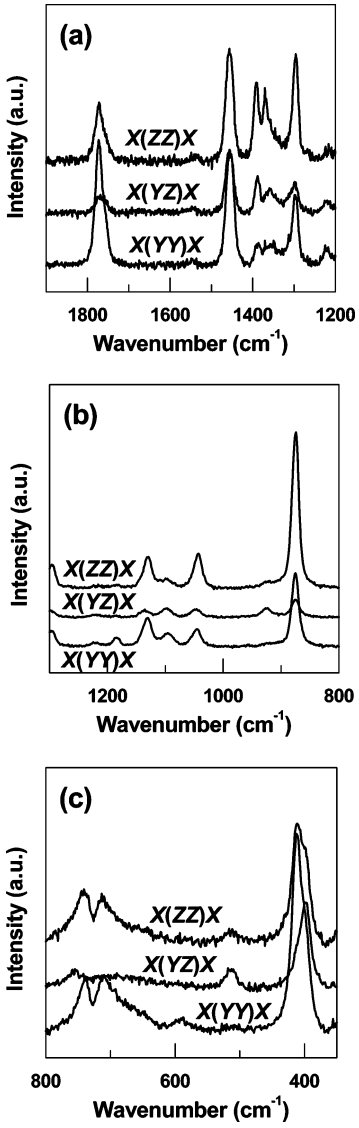

Figure 5. Polarized Raman spectra for area A8 of the necked PLLA film: (a) from 1900 to 1200 cm^{-1}; (b) from 1300 to 800 cm^{-1}; (c) from 800 to 350 cm^{-1}.

Table 4. Ratios of Polarized Raman Scattering Intensities for the Raman Bands at Area A8 of a Uniaxially oriented PLLA Film, Acceptability and Sign of the P_{200} and P_{400} Values, and the Form of Raman Tensor

Raman band (cm^{-1})	tensor form in Table 4	intensity correlation	sign[a] of P_{200}, P_{400}				tensor form: tilt angle (Ω)
			A($k+$)	A($k-$)	E(III)	E(V)	
1777	A	$I_{YY} > I_{ZZ} > I_{YZ}$	+, +	−, +	/	/	A($k+$), A($k-$)
1767	A	overlapped[b]	/	/	/	/	/
1753	A		/	/	/	/	/
1457	E	$I_{YY} > I_{ZZ} > I_{YZ}$	−, +	−, +	−, −	+, N	A($k-$): $\Omega > 45°$
1302	A, E	overlapped	/	/	/	/	/
1295	A, E		/	/	/	/	/
1222	E	$I_{YY} > I_{YZ} \sim I_{ZZ}$	/	/	−, +	+, N	E(V): $\Omega < 45°$
1186	A	$I_{YY} > I_{ZZ} \sim I_{YZ}$	+, +	−, +	/	/	A($k+$), A($k-$)
1133	A	$I_{ZZ} \sim I_{YY} > I_{YZ}$	−, +	+, +	/	/	A($k+$), A($k-$)
1099	A	$I_{YY} > I_{ZZ} \sim I_{YZ}$	N, N	−, −	/	/	A($k-$): $\Omega > 45°$
1047	A	$I_{ZZ} > I_{YY} > I_{YZ}$	−, +	+, +	/	/	A($k+$), A($k-$)
926	E	$I_{YZ} > I_{ZZ} > I_{YY}$	/	/	+, +	N, N	E(III): $\Omega < 45°$
875	A	$I_{ZZ} > I_{YY} > I_{YZ}$	−, N	+, +	/	/	A($k-$): $\Omega < 45°$
740	A	$I_{YY} > I_{ZZ} > I_{YZ}$	+, +	−, +	/	/	A($k+$), A($k-$)
713	A	$I_{YY} > I_{ZZ} > I_{YZ}$	+, +	−, +	/	/	A($k+$), A($k-$)
510	A, E	$I_{YZ} > I_{ZZ} > I_{YY}$	+, N	+, −	+, +	−, N	E(III): $\Omega < 45°$
413	A	$I_{YY} > I_{ZZ} > I_{YZ}$	+, +	−, +	/	/	A($k+$), A($k-$)
398	A, E	$I_{YY} \sim I_{YZ} > I_{ZZ}$	−, −	−, −	−, +	N, N	A(k−): $\Omega > 45°$
347	A	overlapped	/	/	/	/	/

[a] Key: (/) not determined; (N) not acceptable (the value is not within the range of $-0.5 \le P_{200} \le 1$ and $-0.43 \le P_{400} \le 1$). [b] The peak intensity was not obtained due to overlapping of the peak with its neighboring peak.

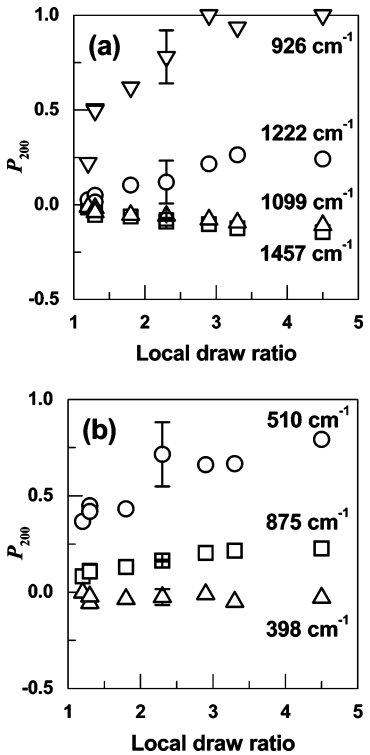

Figure 6. Relationship between local draw ratio and the P_{200} value determined for the Raman bands of the necked PLLA film: regions of (a) high wavenumber or (b) low wavenumber. Error bars are superposed for the plots at DR = 2.3.

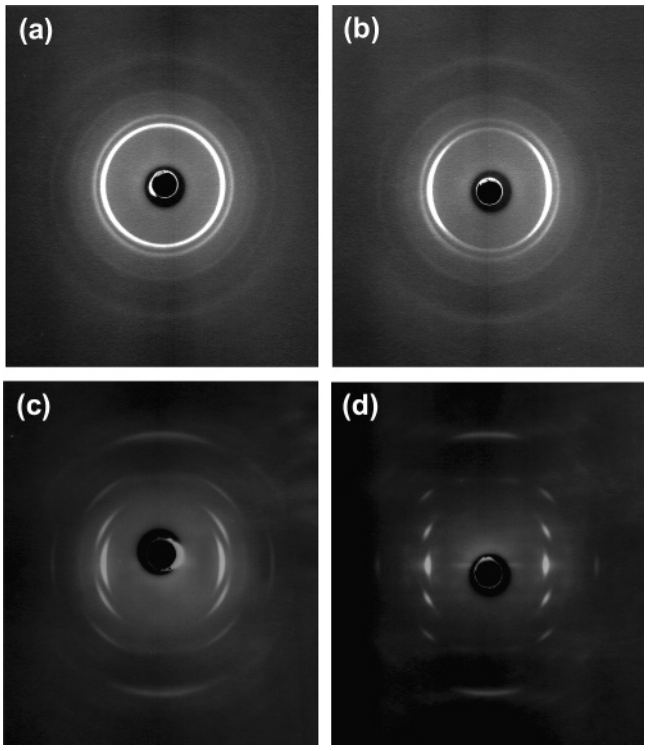

Figure 7. X-ray fiber patterns for the local areas of the necked PLLA film shown in Figure 2: (a) A2, DR = 1.3; (b) A4, DR = 1.8; (c) A6, DR = 2.9, (d) A8; DR = 4.5. The uniaxial drawing direction of the film is vertical.

From the diffraction pattern for the (110) and (200) planes of the PLLA α-form, the crystallite orientation distribution coefficient $P_{200,c}$ was calculated using eqs 13 and 14 for each area of the drawn film. The $P_{200,c}$ values are correlated in Figure 8 with the P_{200} values determined for the Raman bands assigned to the crystalline regions only. The P_{200} value for Raman band at 1222 cm^{-1} was found to be proportional to the $P_{200,c}$ values. Although the P_{200} values for both Raman bands at 926 and 510 cm^{-1} are scattered, they were assumed to be related linearly to the corresponding $P_{200,c}$ value based on eq 3. The tilt angles for these Raman bands could be determined from the slope of their linear correlations using eq 5, as summarized in Table 5.

4.4. Tilt Angle for the Morphology-Independent Raman Bands of PLLA. The tilt angles Ω were also determined for the morphology-independent Raman bands of PLLA at 1457, 1099, 875, and 398 cm^{-1}.

The sample birefringence (Δn) must be known in order to calculate the angle Ω using eq 5. However, it was difficult to measure the Δn values in the necked regions, since the path difference changed not only with the average molecular orientation but also with the sample thickness. Instead, the Δn values for fully uniaxially oriented films with different sample draw ratios were measured. The P_{200} values for the Raman band at 875 cm^{-1} of the uniaxially oriented films are related to their

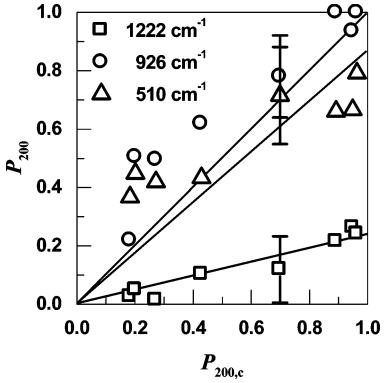

Figure 8. Comparison between the P_{200} values determined for the Raman bands assigned to the crystalline regions only and the $P_{200,c}$ values determined from X-ray fiber patterns for the local areas of the necked PLLA film. Error bars are superposed for the plots at DR = 2.3.

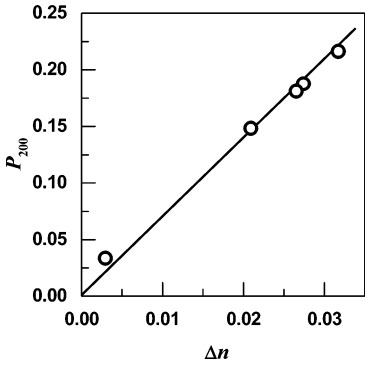

Figure 9. Relationship between the values of sample birefringence for the fully drawn PLLA films with different sample draw ratios and their P_{200} values determined for the Raman band at 875 cm^{-1}.

Table 5. Tilt Angles (Ω) for the Raman Bands of PLLA

assignment	Raman band (cm^{-1})	Ω (deg)
crystalline	1222	45 ± 2
	926	0 ± 21
	510	18 ± 13
morphology-independent	1457	61 ± 0.5
	1099	60 ± 0.2
	875	44 ± 0.3
	398	57 ± 0.3

Δn values in Figure 9, since this Raman band is independent of the morphology of PLLA. The P_{200} value was found to increase in proportion to the Δn value, following an equation of the form,

$$P_{200} = 6.8\Delta n \tag{17}$$

Using this equation the Δn values for the local areas of the drawn film were estimated from their P_{200} values for the 875 cm^{-1} Raman band, and they are given in Table 2.

In addition, the values of intrinsic birefringence for the crystalline (Δn_c) and amorphous regions (Δn_a) of PLLA can be calculated from the following equation:[32,47]

$$\frac{\Delta n}{\chi_c P_{200,c}} = \frac{1-\chi_c}{\chi_c}\frac{P_{200,a}}{P_{200,c}}\Delta n_a + \Delta n_c \tag{18}$$

Data for melt-spun PLLA fibers reported by Schmack et al.[16,17] are shown in Table 6, and eq 18 was applied for these data as shown in Figure 10. From the slope and the intercept of the linear correlation, the Δn_c and Δn_a values for PLLA were determined to be 0.0207 and 0.0587, respectively.

Table 6. Physical Characteristics of Melt-Spun Fibers Studied by Schmack et al.[16,17]

DR	$\Delta n^a \times 10^3$	$\chi_c{}^b$	$P_{200,c}{}^c$	$P_{200,a}{}^d$
4.0	18.04	0.186	0.948	0.459
4.5	19.50	0.197	0.957	0.505
5.0	21.10	0.220	0.967	0.533

[a] Determined by birefringence measurement. [b] Determined by DSC. [c] Determined by WAXD. [d] Determined from the amorphous halo of the WAXD profile.[17]

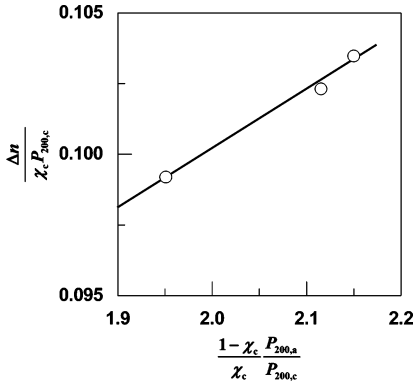

Figure 10. Relationship in eq 18 for the data obtained from melt-spun PLLA fibers reported by Schmack et al.[16,17]

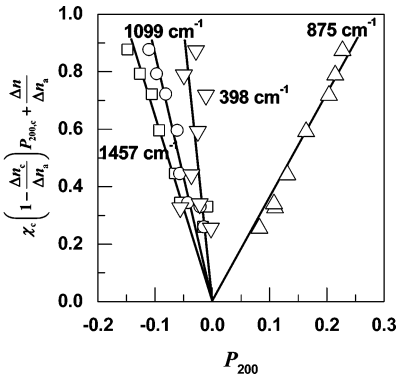

Figure 11. Correlations given by eq 5 for the necked PLLA film with respect to the morphology-independent Raman bands.

For each Raman band, the right-hand term in eq 5 is plotted against the P_{200} value for each local area of the drawn film in Figure 11. The plots show a linear correlation that extrapolates to the origin for all the Raman bands. Their tilt angles Ω were calculated from the slopes of the correlations, and are given in Table 5.

4.5. Deformation Model for the Crystalline and Amorphous Regions of the PLLA Film During Uniaxial Deformation. Now that the tilt angles for the morphology-independent Raman bands are known, it was possible to determine the $P_{200,chain}$ value for each area of the drawn PLLA film by using eq 3.

Figure 12 shows the relationship between the local draw ratio and the $P_{200,chain}$ value obtained from each Raman band. The $P_{200,chain}$ value increased with an increase of the local draw ratio, and the results were consistent for all the Raman bands except for the 398 cm^{-1} band. The large scatter of the data for the 398 cm^{-1} band was considered due to its high tilt angle of 56.9°. In eq 3, the coefficient of the P_{200} value is divergent at Ω = 54.7°; hence, a small discrepancy in the measurement of the P_{200} value for the 398 cm^{-1} band could cause a significant error for the determination of the angle Ω and the $P_{200,chain}$ value.

The second order of the orientation distribution coefficient for the amorphous regions ($P_{200,a}$) was calculated using eq 6

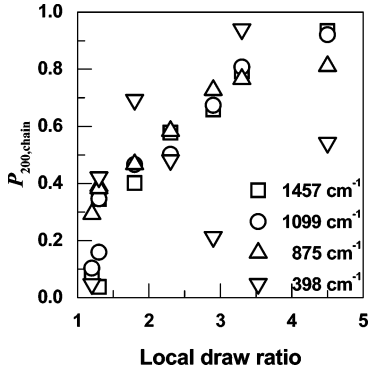

Figure 12. Relationships between local draw ratios and the $P_{200,chain}$ values for the necked PLLA film determined by polarized Raman spectroscopy.

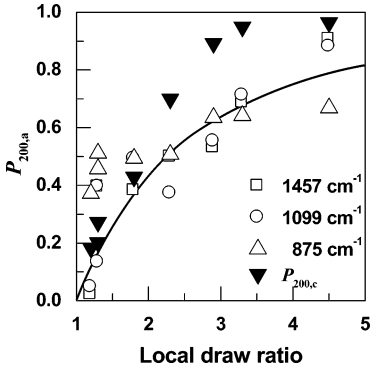

Figure 13. Relationships between local draw ratios and the $P_{200,a}$ values for the necked PLLA film determined by polarized Raman spectroscopy. The $P_{200,c}$ values and a P_{200} curve based on pseudo-affine deformation model, $P_{200,p-aff}$, are superposed.

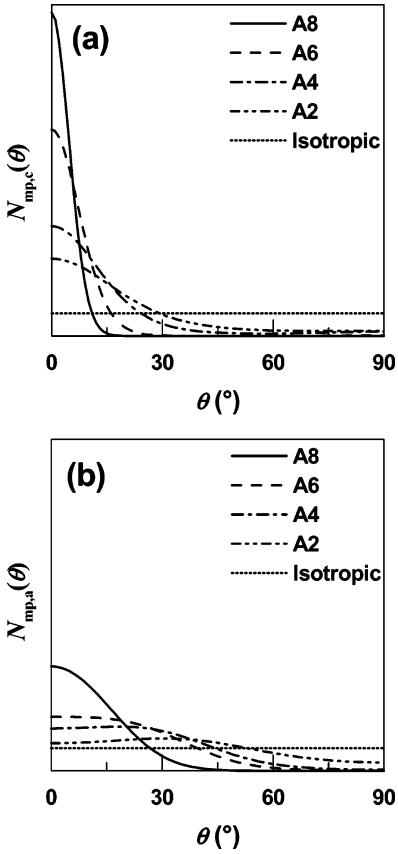

Figure 14. Molecular orientation distribution functions ($N_{mp}(\theta)$) in the (a) crystalline and (b) amorphous regions for the local areas of the necked PLLA film. The angle $\theta = 0°$ corresponds to the direction of sample drawing.

for each local area of the drawn PLLA film, and is shown in Figure 13. Because of the lack of accuracy of the P_{200} value for the 398 cm^{-1} Raman band, the results are given only for the Raman bands at 1457, 1099, and 875 cm^{-1}. Although the $P_{200,a}$ values were shown to be more scattered in the areas with lower local draw ratios, the $P_{200,a}$ values determined from each Raman band are reasonably comparable with each other. The $P_{200,c}$ values for the corresponding areas of the drawn PLLA film are also superposed in Figure 13. It can be seen that the molecular orientation in the crystalline regions was highly developed at a draw ratio around 3.5. In contrast, the development of molecular orientation in the amorphous regions was found to be slower than that in the crystalline regions.

The most probable molecular orientation distribution functions $N_{mp}(\theta)$ for both the crystalline and amorphous regions were further determined using the corresponding coefficients P_{200} and P_{400}. The $P_{200,c}$ and $P_{400,c}$ values at each area of the sample were calculated from averaging the values for the Raman bands at 1222, 926, and 510 cm^{-1} using eq 3. The $P_{200,a}$ values were, on the other hand, calculated from an average of those for the Raman bands at 1457, 1099, and 875 cm^{-1} in Figure 13, and the $P_{400,a}$ value was estimated using eq 7. These P_{200} and P_{400} values were employed to determine the coefficients A_{l00}^{mp} using eqs 9 and 10 for both the crystalline and amorphous regions. The results are summarized in Table 7.

Parts a and b of Figure 14 show the most probable molecular orientation distribution functions for the crystalline ($N_{mp,c}(\theta)$) and amorphous regions ($N_{mp,a}(\theta)$), respectively, for the local areas of the drawn PLLA film. For clarity, the functions are shown only for the areas A2, A4, A6, and A8, and they are compared to that of an isotropic distribution. In Figure 14a, the function $N_{mp,c}(\theta)$ increased its height at $\theta = 0°$ with increasing the local draw ratio, while the peak width became narrower. Since the angle $\theta = 0°$ corresponds to the axis of sample drawing, this indicates that the molecules were oriented more toward the drawing direction. In contrast, the molecular orientation distributions in the amorphous regions shown in Figure 14b were much broader than those in the crystalline regions.

Table 7. Molecular Orientation Distribution Coefficients P_{l00} and the Corresponding Coefficients A_{l00}^{mp} for Both the Crystalline and Amorphous Regions at Local Areas of the Uniaxially Oriented PLLA Film

		crystalline				amorphous			
area	DR	$P_{200,c}$	$P_{400,c}$	$A_{200,c}^{mp}$	$A_{400,c}^{mp}$	$P_{200,a}$	$P_{400,a}$	$A_{200,a}^{mp}$	$A_{400,a}^{mp}$
A1	1.2	0.253	0.260	0.592	1.663	0.147	−0.039	0.759	−0.442
A2	1.3	0.413	0.203	1.497	0.732	0.193	−0.043	1.017	−0.553
A3	1.3	0.349	0.515	−0.071	4.185	0.416	0.008	2.452	−0.950
A4	1.8	0.519	0.376	1.421	1.710	0.456	0.031	2.768	−1.002
A5	2.3	0.706	0.643	1.091	3.855	0.459	0.033	2.802	−1.012
A6	2.9	0.892	0.799	1.534	5.643	0.573	0.128	3.851	−1.128
A7	3.3	0.905	0.869	−0.378	10.10	0.680	0.261	5.331	−1.261
A8	4.5	0.933	0.902	14.12	10.85	0.819	0.509	8.648	−1.321

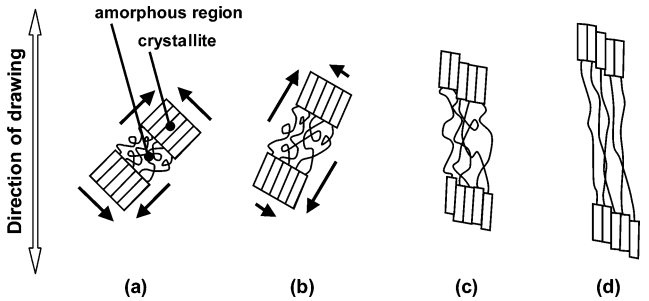

Figure 15. Deformation model for the crystallites and amorphous regions of the PLLA film during uniaxial drawing: (a) an initial stage (DR = 1); (b) stage I (DR = 1−2) where the shear stress is below the CRSS; (c) stage II (DR = 2−3.5) where the shear stress is above the CRSS; (d) stage III (DR > 3.5). Arrows indicate the directions of shear stresses.

The development of molecular orientation in a material during its uniaxial deformation can be described by using the so-called *pseudo-affine* deformation model.[67,68] This model, developed originally for rubber, was considered to be suitable for the current sample, where plastic flow of the material might occur for high strain deformation. According to the pseudo-affine deformation model, the orientation angles of a unit before (Θ) and after uniaxial drawing (Θ') can be related[69] to each other with respect to the sample draw ratio, Λ, by

$$\tan \Theta = \Lambda^{3/2} \tan \Theta' \tag{19}$$

On the other hand, sample birefringence can be related[67] to the intrinsic birefringence of the sample, Δn_o, and the value Λ by

$$\Delta n = \frac{\Delta n_o}{2}\left[\frac{3}{1-\Lambda^{-3}} - \frac{3\Lambda^{-3/2}\cos^{-1}\Lambda^{-3/2}}{(1-\Lambda^{-3})^{3/2}} - 1\right] \tag{20}$$

where the Δn_o value is regarded as the sample birefringence for perfect molecular orientation, which may be determined by

$$\Delta n_o = \chi_c \Delta n_c + (1-\chi_c)\Delta n_a \tag{21}$$

Using eqs 6 and 21, eq 20 can be arranged to give the P_{200} value for the pseudo-affine deformation model, $P_{200,p-aff}$, as

$$P_{200,p-aff} = \frac{1}{2}\left[\frac{2\Lambda^3+1}{\Lambda^3-1} - \frac{3\Lambda^3\cos^{-1}\Lambda^{-3/2}}{(\Lambda^3-1)^{3/2}}\right] \tag{22}$$

A curve of the $P_{200,p-aff}$ values calculated using eq 22 was superposed with those determined by polarized Raman spectroscopy in Figure 13. The $P_{200,a}$ values were consistent with the $P_{200,p-aff}$ curve. This suggests that the development of molecular orientation in the amorphous regions of the PLLA film follows the pseudo-affine deformation mechanism during uniaxial drawing. On the other hand, the $P_{200,c}$ values follows the $P_{200,p-aff}$ curve at DR < 2. Above this local draw ratio, the $P_{200,c}$ value increased more rapidly than the $P_{200,p-aff}$ value. This deviation of the $P_{200,c}$ value from the $P_{200,p-aff}$ value may be explained by considering the occurrence of crystal rotation and crystal slip[70−72] as shown schematically in Figure 15.

When the PLLA film is stretched, crystal lamellae experience a longitudinal tensile stress, which causes shear stresses in the lamellar structure (Figure 15a). This initial stage corresponds to DR = 1 in Figure 13. As the drawing progresses, the crystallites rotate to reduce the shear stress built-up, meanwhile the molecules in the amorphous regions are elongated following the pseudo-affine deformation mechanism (stage I, DR = 1−2, Figure 15b). When the amount of the shear stress exceeds the so-called *critical resolved shear stress*[70] (CRSS), which is the lowest stress to cause slip in the crystallites on a certain crystal plane, the shear stress built-up will be relieved by crystallite slip. The crystallite slip and rotation promote rapid orientation of crystallites toward the film drawing direction (stage II, DR = 2−3.5, Figure 15c), while the amorphous regions continue with pseudo-affine deformation. As a result, the crystallites could become highly oriented by DR = 3.5, and the molecular orientation in the amorphous regions still progresses at higher local draw ratios (Stage III, DR > 3.5, Figure 15d).

5. Conclusions

Molecular orientation distributions in the crystalline and amorphous regions were studied for a drawn PLLA film by means of polarized Raman spectroscopy. Raman bands of PLLA were assigned as being either from the crystalline regions only or as being morphology independent by analyzing their temperature dependence. The tensor forms of the Raman bands were determined by comparing their relative intensities in polarized Raman spectra based on the assumption that all the bands have cylindrical symmetry.

Raman bands at 1222, 926, and 510 cm^{-1} were suitable for the study of molecular orientation distributions in the crystalline regions only. The tilt angle Ω was determined from the second order of the molecular orientation distribution coefficient P_{200} for each Raman band in association with the results of WAXD. It was possible to derive the P_{200} value for the crystalline regions ($P_{200,c}$) after correcting the P_{200} value for the Raman band for its tilt angle Ω.

The Raman bands at 1457, 1099, 875, and 398 cm^{-1} were studied closely in order to determine the molecular orientation distribution coefficients in the amorphous regions. The tilt angle Ω for each Raman band was determined in combination with the results of birefringence measurements, which enabled the P_{200} values for an average of molecules in the crystalline and amorphous regions ($P_{200,chain}$) to be calculated, in addition to those in the amorphous regions only ($P_{200,a}$). At a local draw ratio of above 2, molecular orientation in the crystalline regions was found to progress more rapidly than in the amorphous regions. This is considered due to the occurrence of crystallite slip and rotation, while the molecules in the amorphous regions are stretched under the pseudo-affine deformation.

Both the P_{200} and P_{400} values for the Raman bands assigned to the crystalline regions only were corrected for their tilt angle Ω in order to determine the most probable molecular orientation distribution functions $N_{mp}(\theta)$ for the crystalline regions. By estimating the P_{400} value for the amorphous regions by only using the $P_{200,a}$ value, it was possible to determine the functions $N_{mp}(\theta)$ for the amorphous regions only. It was found that PLLA molecules in the crystalline regions were oriented preferentially toward the film drawing direction even at a low draw ratio of around 2. In contrast, the molecular orientation in the amorphous regions was shown to be much less significant than that in the crystalline regions. The result suggests that successful molecular orientation in the amorphous regions of the PLLA film may only be achieved when the film is stretched to draw ratios above 4.5.

Acknowledgment. The work was supported by Four Square, a Division of Mars U.K., Ltd. One of the authors (M.T.) is grateful to Universities UK for financial support through the ORS scheme (ORS/2000028028).

References and Notes

(1) Sinclair, R. G. *J. Macromol. Sci.—Pure Appl. Chem.* **1996**, *A35*, 585.
(2) Bogaert, J.-C.; Coszach, P. *Macromol. Symp.* **2000**, *153*, 287.

(3) Dorgan, J. R.; Lehermeier, H.; Palade, L.-I.; Cicero, J. *Macromol. Symp.* **2001**, *175*, 55−66.
(4) Li, S. M.; Garreau, H.; Vert, M. *J. Mater. Sci.: Mater. Med.* **1990**, *1*, 123.
(5) Roten-Weinhold, A.; Besseghir, K.; Vuaridel, E.; Sublet, E.; Oudry, N.; Kubel, F.; Gurny, R. *Eur. J. Pharmaceut. Biopharmaceut.* **1999**, *48*, 113−121.
(6) Hyon, S.-H.; Jin, F.; Jamshidi, K.; Tsutsumi, S.; Kanamoto, T. *Macromol. Symp.* **2003**, *197*, 355−368.
(7) Tsuji, H.; Ikada, Y. *Polym.* **1995**, *36*, 2709.
(8) Cai, H.; Dave, V.; Gross, R. A.; McCarthy, S. P. *J. Polym. Sci., Part B: Polym. Phys. Ed.* **1996**, *34*, 2701−2708.
(9) Iannace, S.; Maffezzoli, A.; Leo, G.; Nicolais, L. *Polym.* **2001**, *42*, 3799.
(10) Smith, P. B.; Leugers, A.; Kang, S.; Hsu, S. L.; Yang, X. *J. Appl. Polym. Sci.* **2001**, *82*, 2497−2505.
(11) Burg, K. J. L.; LaBerge, M.; Shalaby, S. W. *Biomaterials* **1998**, *19*, 785−789.
(12) Roe, R. J.; Krigbaum, W. R. *J. Appl. Phys.* **1964**, *35*, 2215−2219.
(13) Roe, R.-J.; Krigbaum, W. R. *J. Chem. Phys.* **1964**, *40*, 2608−2615.
(14) Roe, R.-J. *J. Appl. Phys.* **1965**, *36*, 2024−2031.
(15) Ohkoshi, Y.; Shirai, H.; Gotoh, Y.; Nagura, M. *Sen'i Gakkaishi* **1998**, *55*, 21.
(16) Schmack, G.; Taendler, B.; Vogel, R.; Beyreuther, R.; Jacobsen, S.; Fritz, H.-G. *J. Appl. Polym. Sci. Lett.* **1999**, *73*, 2785.
(17) Schmack, G.; Jehnichen, D.; Vogel, R.; Taendler, B.; Beyreuther, R.; Jacobsen, S.; Fritz, H.-G. *J. Biotechnol.* **2001**, *86*, 151.
(18) Okuzaki, H.; Kubota, I.; Kunugi, T. *J. Polym. Sci., Part B: Polym. Phys. Ed.* **1999**, *37*, 991.
(19) Lim, J. Y.; Kim, S. H.; Lim, S.; Kim, Y. H. *Macromol. Chem. Phys.* **2001**, *202*, 2447−2453.
(20) Lim, J. Y.; Kim, S. H.; Lim, S.; Kim, Y. H. *Macromol. Mater. Eng.* **2003**, *288*, 50−57.
(21) Ito, T.; Maruhashi, Y.; Demura, M.; Asakura, T. *Polymer* **2000**, *41*, 859−866.
(22) McBrierty, V. J.; Ward, I. M. *Brit. J. Appl. Phys.* **1968**, *1*, 1529−1542.
(23) Clayden, N. J.; Eaves, J. G.; Croot, L. *Polymer* **1997**, *38*, 159−163.
(24) Sawai, D.; Takahashi, K.; Sasashige, A.; Kanamoto, T.; Hyon, S.-H. *Macromolecules* **2003**, *36*, 3601−3605.
(25) Smith, P. B.; Leugers, A.; Kang, S.; Yang, X.; Hsu, S. L. *Macromol. Symp.* **2001**, *175*, 81−94.
(26) Tanaka, M.; Young, R. J. *J. Mater. Sci.* **2006**, *41*, 963−994.
(27) Cunningham, A.; Davies, G. R.; Ward, I. M. *Polymer* **1974**, *15*, 743−748.
(28) Bower, D. I. *J. Polym. Sci.: Polym. Phys. Ed.* **1972**, *10*, 2135−2153.
(29) Sourisseau, C. *Chem. Rev.* **2004**, *104*, 3851−3891.
(30) Bower, D. I. *J. Polym. Sci.: Polym. Phys. Ed.* **1981**, *19*, 93−107.
(31) Pigeon, M.; Prud'homme, R. E.; Pezolet, M. *Macromolecules* **1991**, *24*, 5687−5694.
(32) Tanaka, M.; Young, R. J. *J. Macromol. Sci. Phys.-B* **2005**, *44*, 967−991.
(33) Hoogsteen, W.; Postema, A. R.; Pennings, A. J.; ten Brinke, G.; Zugenmaier, P. *Macromolecules* **1990**, *23*, 634.
(34) Kobayashi, J.; Asahi, T.; Ichiki, M.; Oikawa, A.; Suzuki, H.; Watanabe, T.; Fukada, E.; Shikinami, Y. *J. Appl. Phys.* **1995**, *77*, 2957.
(35) Fraser, G. V.; Hendra, P. J.; Watson, D. S.; Gall, M. J.; A.Willis, H.; Cudby, M. E. A. *Spectrochim. Acta* **1973**, *29A*, 1525−1533.
(36) Bower, D. I. *J. Phys. B: Atom. Mol. Phys.* **1976**, *9*, 3275−3293.
(37) Purvis, J.; Bower, D. I. *J. Polym. Sci.: Polym. Phys. Ed.* **1976**, *14*, 1461−1484.
(38) Lovell, R.; Mitchell, G. R. *Acta Crystallogr.* **1981**, *A37*, 135−137.
(39) Everall, N. J. *Appl. Spectrosc.* **1998**, *52*, 1498−1504.
(40) Rousseau, M.-E.; Lefevre, T.; Beaulieu, L.; Asakura, T.; Pezolet, M. *Biomacromolecules* **2004**, *5*, 2247−2257.
(41) Ward, I. M. *Mechanical Properties of Solid Polymers*, 2nd ed.; John Wiley & Sons: Chichester, U.K., 1983.
(42) Kister, G.; Cassanas, G.; Vert, M.; Pauvert, B.; Terol, A. *J. Raman Spectrosc.* **1995**, *26*, 307.
(43) Kister, G.; Cassanas, G.; Vert, M. *Polymer* **1998**, *39*, 267.
(44) Kang, S.; Hsu, S. L.; Stidham, H. D.; Smith, P. B.; Leugers, M. A.; Yang, X. *Macromolecules* **2001**, *34*, 4542−4548.
(45) Alexander, L. E. *X-ray Diffraction Methods in Polymer Science*; Wiley-Interscience: John Wiley & Sons: New York, 1969.
(46) Nomura, S.; Kawai, H.; Kimura, I.; Kagiyama, M. *J. Polym. Sci., Part A-2* **1970**, *8*, 383−400.
(47) Samuels, R. J. *J. Polym. Sci., Part A* **1965**, *3*, 1741−1763.
(48) Satija, S. K.; Wang, C. H. *J. Chem. Phys.* **1978**, *69*, 2739−2744.
(49) Stein, R. S.; Norris, F. H. *J. Polym. Sci.* **1956**, *21*, 381−396.
(50) Nomura, S.; Nakamura, N.; Kawai, H. *J. Polym. Sci., Part A-2* **1971**, *9*, 407−420.
(51) Windle, A. H. In *Developments in Oriented Polymers-1*; Ward, I. M., Ed.; Applied Science Publishers: London, 1982; pp 1−46.
(52) Ward, I. M. In *Adv. Polym. Sci.*; Kausch, H. H.; Zachmann, H. G., Eds.; Springer-Verlag: Berlin, 1985; Vol. 66, pp 81−115.
(53) Berne, B. J.; Pechukas, P.; Harp, G. D. *J. Chem. Phys.* **1968**, *49*, 3125−3129.
(54) Pottel, H.; Herreman, W.; Meer, B. W. van der; Ameloot, M. *Chem. Phys.* **1986**, *102*, 37−44.
(55) Lewis, E. L. V.; Bower, D. I.; Ward, I. M. *Polym.* **1995**, *36*, 4741−4752.
(56) Bremard, C.; Dhamelincourt, P.; Laureyns, J.; Turrell, G. *Appl. Spectrosc.* **1985**, *39*, 1036−1039.
(57) Bremard, C.; Dhamelincourt, P.; Laureyns, J.; Turrell, G. *J. Mol. Struct.* **1986**, *142*, 13−16.
(58) Bremard, C.; Laureyns, J.; Turrell, G. *Can. J. Spectrosc.* **1987**, *32*, 70−78.
(59) Everall, N.; Owen, H.; Slater, *J. Appl. Spectrosc.* **1995**, *49*, 610−615.
(60) Damen, T. C.; Porto, S. P. S.; Tell, B. *Phys. Rev.* **1966**, *142*, 570−574.
(61) Hammersley, A. The Fit2D Home Page, 2004 ESRF, www.esrf.fr/computing/scientific/FIT2D/.
(62) Fischer, E. W.; Sterzel, H. J.; Wegner, G. *Kolloid-Z. Z. Polym.* **1973**, *251*, 980−990.
(63) Cai, H.; Dave, V.; Gross, R. A.; McCarthy, S. P. *J. Polym. Sci., Part B: Polym. Phys. Ed.* **1996**, *34*, 2701−2708.
(64) Lee, J. K.; Lee, K. H.; Jin, B. S. *Eur. Polym. J.* **2001**, *37*, 907−914.
(65) Jamshidi, K.; Hyon, S.-H.; Ikada, Y. *Polymer* **1988**, *29*, 2229.
(66) Qin, D.; Kean, R. T. *Appl. Spectrosc.* **1998**, *52*, 488−495.
(67) Crawford, S. M.; Kolsky, H. *Proc. Phys. Soc. (London)* **1951**, *B64*, 119−125.
(68) Ward, I. M. *Mechanical Properties of Solid Polymers*, 2nd ed.; John Wiley & Sons: Chichester, 1983.
(69) Kratky, Von O. *Kolloid-Z.* **1933**, *64*, 213−222.
(70) Bowden, P. B.; Young, R. J. *J. Mater. Sci.* **1974**, *9*, 2034−2051.
(71) Pope, D. P.; Keller, A. *J. Polym. Sci.: Polym. Phys. Ed.* **1975**, *13*, 533−566.
(72) Hiss, R.; Hobeika, S.; Lynn, C.; Strobl, G. *Macromolecules* **1999**, *32*, 4390−4403.

MA0526286